Fully and double differential cross sections for the single ionization of H_2O by bare ion impact

2014 J. Phys. B: At. Mol. Opt. Phys. 47 035205

(http://iopscience.iop.org/0953-4075/47/3/035205)

IOP Publishing Journal of Physics B: Atomic, Molecular and Optical Physics
J. Phys. B: At. Mol. Opt. Phys. **47** (2014) 035205 (11pp) doi:10.1088/0953-4075/47/3/035205

Fully and double differential cross sections for the single ionization of H_2O by bare ion impact

L Fernández-Menchero[1,2] **and S Otranto**[3]

[1] Atomic Data and Analysis Structure, Department of Physics, University of Strathclyde, UK
[2] Max-Planck-Institut für Plasmaphysik, Boltzmannstraße 2, D-85748 Garching, Germany
[3] IFISUR and Departamento de Física, Universidad Nacional del Sur, Av. Alem 1253, 8000 Bahía Blanca, Argentina

E-mail: luis.fernandez-menchero@strath.ac.uk

Received 13 November 2013, revised 10 December 2013
Accepted for publication 23 December 2013
Published 21 January 2014

Abstract
A theoretical study of fully differential cross sections for the single ionization of H_2O by collisions with H^+, $\bar{p}^-$ and He^{2+} at an impact energy of 2 and 6 MeV amu^{-1} is presented. We work in terms of the Born-3DW model, which considers in the final state a model central potential to represent the interaction of the emitted electron with the molecular core. Results are presented for the lesser bound molecular orbitals ($1B_1$, $1B_2$, $2A_1$ and $3A_1$). Doubly differential cross sections in terms of the electron emission angle are also presented for these molecular orbitals, showing a nearly isotropic distribution for the electron energies under consideration.

Keywords: atomic structure, ion–molecule collisions, ionization

(Some figures may appear in colour only in the online journal)

1. Introduction

Ionization of atoms and molecules by fast charged particles has been a matter of active research in the last two decades [1]. This could be partially due to the natural desire of increasing our understanding of the physics underlying in simple collision systems. It should be noted that at the fully differential level, collision processes involving the simplest possible targets (H and He) remained elusive at low impact energies until the last decade when numerically intensive methods provided what could be defined as definite cross sections for (e,2e) processes (see [2–4] and references therein). Besides, atomic processes are also relevant in many areas, like atmosphere physics, (fusion) plasma and astrophysics, for which there is a need of cross sections concerning charge exchange and ionization processes originated by charged particle impact. Those cross sections can be ulteriorly used to feed statistical models which track the energy deposition of a particle as it enters into the target area of interest. In this sense, ionization cross sections for ion impact on biological molecules could be useful in biology and medicine, in areas like radiobiology, medical imaging and radiotherapy as well [5]. It is worth noting that ion therapy has been raised in recent years as a potential technique for treating cancer tumours and several facilities are currently underway like those at Heidelberg, Pavia, Marburg and Kiel.

From the experimental point of view, and starting in the mid-1990s, the development of the cold target recoil ion momentum spectroscopy (COLTRIMS) [6–8] technique, has provided a new insight on collision systems since it allowed kinematically complete experiments of collision processes involving photons, ions, and electrons to be performed [9–12]. Following the Frankfurt and Heidelberg groups, this technique has since then been adopted by several laboratories worldwide. Despite the limitations in the experimental setup (only low-energy emitted electrons are detected to avoid prohibitive extraction fields), a vast amount of data has been obtained for a large variety of collision systems. More recent works have been realized in ion–atom [13–16], ion–molecule [17–21], and ion–cluster [22] collisions.

Theoretically, fully differential cross sections (FDCSs) in ion–atom collisions have been calculated by means of continuum distorted wave (CDW) models [23–31], by the classical trajectory Monte Carlo method (CTMC) [32–36], or applying other approximated methods [37–40] for which this work could be a good testing reference. FDCS in ion–molecule collisions have been studied in terms of a Born-3DW model, assuming that the molecular potential is either purely Coulombic [41, 42], or a central potential which takes into account the multielectronic character of the resulting molecular ion [43, 44].

In a previous work [43], we presented the Born-3DW method to obtain the FDCS for single ionization of the CH_4 molecule by bare ion impact for impact energies in the order of MeV amu^{-1}. In this work, we consider the single ionization of the water molecule by fully stripped ions at high impact energies. We also integrate the FDCS in the projectile deflection angles and calculate the double differential cross sections (DDCSs) as a function of the electron emission angle. This target is of particular interest in astrophysics (largely populates cometary comas and planetary atmospheres), in radiobiology (where the water molecule resembles organic matter), or in fusion plasmas (where oxygen atoms are used for diagnosis and can react with the hydrogen forming at most water, and other species, like H_3O^+, OH^- or H_2O_2 in the cold zones of the plasma, like the divertors).

The paper is organized as follows: the next section is devoted to a brief description of the theoretical model in use. In section 3, we analyze the FDCS calculated in this work for the single ionization of water by H^+, $\bar{p}^-$ and He^{2+} impact and the DDCS for the impact with alpha particle. In section 4, we draw our conclusions and outlook. Atomic units are used throughout this work unless otherwise stated.

2. Theoretical model

We consider a stripped ion of charge Z_P and mass M_P incident upon a multielectron molecular target of mass M_T in the ground state. We consider one active electron placed in the molecular orbital i of the ground state, so the initial wave function for the target can be written as $\phi_i(\boldsymbol{r})$. This wave function is an eigenfunction of the Schrödinger equation with a molecular model potential $V_{\mathrm{mol}i}(\boldsymbol{r})$, which includes the nuclei and the other electron terms:

$$V_{\mathrm{mol}i}(\boldsymbol{r}) = -\sum_{l=1}^{M}\frac{Z_l}{|\boldsymbol{r}-\boldsymbol{R}_l|} + \sum_{j=1}^{N_{\mathrm{MO}}} N_{ij}\int \mathrm{d}^3\boldsymbol{r}'\frac{|\phi_j(\boldsymbol{r}')|^2}{|\boldsymbol{r}-\boldsymbol{r}'|}, \quad (1)$$

where M is the number of nuclei which form the molecule, Z_l the charge each nuclei, $\boldsymbol{R}_l$ their position with respect to the molecular centre of mass, N_{MO} the number of molecular orbitals of the molecule and N_{ij} values 2 if $i \neq j$, and 1 if $i = j$, and $\phi_j(\boldsymbol{r}')$ their one-electron wave functions. Following the steps of [43], we use the SCF-MO analytical expansions in terms of Slater functions provided by Moccia [45] for the five occupied orbitals of H_2O in its ground state: $1A_1$, $2A_1$, $3A_1$, $1B_2$ and $1B_1$. As the inner orbital $1A_1$ is tightly bound (−20.5249 au), we neglect its contribution to the ionization channel. The binding energies employed throughout this work are −1.3261, −0.5561, −0.6814 and −0.4954 au for the $2A_1$, $3A_1$, $1B_2$ and $1B_1$ molecular orbitals, respectively.

Table 1. Coefficients of the expansion of the wave function of the orbital $2A_1$ of H_2O. $E = -1.3261$ au.

l, m	0, 0			1, 0		
a, n, ξ	0.01889	1	12.600	0.02484	2	3.920
	−0.255 92	1	7.450	−0.008 35	2	2.440
	0.099 39	2	3.240	0.186 36	2	1.510
	0.777 45	2	2.200			
	0.163 59	2	1.280			
l, m	2, 0			3, 0		
a, n, ξ	0.002 15	3	2.400	−0.026 28	4	1.950
	0.006 95	3	1.600			
l, m	2, 2			2, −2		
a, n, ξ	−0.006 99	3	2.400	−0.006 99	3	2.400
	−0.045 28	3	1.600	−0.045 28	3	1.600
l, m	3, 2			3, −2		
a, n, ξ	−0.039 88	4	1.950	−0.039 88	4	1.950

Table 2. Coefficients of the expansion of the wave function of the orbital $3A_1$ of H_2O. $E = -0.5561$ au.

l, m	0, 0			1, 0		
a, n, ξ	−0.008 48	1	12.600	0.244 13	2	3.920
	0.082 41	1	7.450	0.004 83	2	2.440
	−0.041 32	2	3.240	0.799 79	2	1.510
	−0.307 52	2	2.200			
	0.149 54	2	1.280			
l, m	2, 0			3, 0		
a, n, ξ	0.003 96	3	2.400	−0.019 29	4	1.950
	0.059 35	3	1.600			
l, m	2, 2			2, −2		
a, n, ξ	0.012 06	3	2.400	0.012 06	3	2.400
	−0.065 71	3	1.600	−0.065 71	3	1.600
l, m	3, 2			3, −2		
a, n, ξ	−0.046 62	4	1.950	−0.046 62	4	1.950

In the list of Moccia coefficients, we obtain the pairs (l, m) that contribute to the cross section for each molecular orbital and the parameters for these radial expansions in Slater functions a, n, ξ as follows:

$$\phi_i(\boldsymbol{r}) = \sum_{lm}\sum_{j=1}^{k} a_{lmij}\mathcal{R}_{n_{ij}\xi_{ij}}(r)Y_{lm}(\hat{\boldsymbol{r}}), \quad (2)$$

where $\mathcal{R}_{n_{ij}\xi_{ij}}(r)$ are the Slater functions given by

$$\mathcal{R}_{n\xi}(r) = \sqrt{\frac{(2\xi)^{2n+1}}{(2n)!}}\,\mathrm{e}^{-\xi r}\,r^{n-1}. \quad (3)$$

The expansion coefficients are shown in tables 1–4. This expansion corresponds to a basis set of complex spherical harmonics Y_{lm} and not real ones C_{lm}, S_{lm}, as shown directly in [45]. Hence, the coefficients for $m \neq 0$ differ in a factor $\sqrt{2}$ and i imaginary unit.

The transition amplitude for single ionization can be written as

$$T_{fi} = \langle \Psi_f \,|\, V_1 \,|\, \Psi_i \rangle, \quad (4)$$

where the initial channel wave function $\Psi_i(\boldsymbol{K}_i; \boldsymbol{R}_i, \boldsymbol{r})$ is given by the wave function for the molecular orbital under consideration times an incident plane-wave for the incoming projectile:

Table 3. Coefficients of the expansion of the wave function of the orbital $1B_2$ of H_2O. $E = -0.6814$ au.

l, m	1, 1			1, −1		
a, n, ξ	$0.163\,97\,i$	2	3.920	$0.163\,97\,i$	2	3.920
	$-0.050\,08\,i$	2	2.440	$-0.050\,08\,i$	2	2.440
	$0.624\,16\,i$	2	1.510	$0.624\,16\,i$	2	1.510
l, m	2, 1			2, −1		
a, n, ξ	$-0.014\,04\,i$	3	2.400	$-0.014\,04\,i$	3	2.400
	$0.179\,92\,i$	3	1.600	$0.179\,92\,i$	3	1.600
l, m	3, 1			3, −1		
a, n, ξ	$0.032\,00\,i$	4	1.950	$0.032\,00\,i$	4	1.950
l, m	3, 3			3, −3		
a, n, ξ	$-0.045\,12\,i$	4	1.950	$-0.045\,12\,i$	4	1.950

Table 4. Coefficients of the expansion of the wave function of the orbital $1B_1$ of H_2O. $E = -0.4954$ au.

l, m	1, 1			1, −1		
a, n, ξ	0.175 78	2	3.920	−0.175 78	2	3.920
	0.081 54	2	2.440	−0.081 54	2	2.440
	0.509 69	2	1.510	−0.509 69	2	1.510
l, m	2, 1			2, −1		
a, n, ξ	0.002 85	3	2.400	−0.002 85	3	2.400
	0.038 70	3	1.600	−0.038 70	3	1.600
l, m	3, 1			3, −1		
a, n, ξ	0.006 61	4	1.950	−0.006 61	4	1.950
l, m	3, 3			3, −3		
a, n, ξ	−0.019 03	4	1.950	0.019 03	4	1.950

$$\Psi_i = \frac{1}{(2\pi)^{3/2}} \mathrm{e}^{\mathrm{i}\boldsymbol{K}_i\cdot\boldsymbol{R}_i}\phi_i(\boldsymbol{r}). \tag{5}$$

Here, $\boldsymbol{R}_i$ is the relative coordinate between the projectile and the centre of mass of the target molecule before the collision. The final channel wave function $\Psi_f(\boldsymbol{K}_f; \boldsymbol{R}_f, \boldsymbol{r})$ is written as

$$\Psi_f = \frac{1}{(2\pi)^{3/2}} \mathrm{e}^{\mathrm{i}\boldsymbol{K}_f\cdot\boldsymbol{R}_f} C^-(\boldsymbol{K}_f; \boldsymbol{R}_f) \times \chi^-(\boldsymbol{k}; \boldsymbol{r}) C^-(\boldsymbol{k}_{e\mathrm{P}}; \boldsymbol{R}_f - \boldsymbol{r}), \tag{6}$$

where $\boldsymbol{r}$ is the coordinate of the ejected electron with respect to the centre of mass of the ionized target system, $\boldsymbol{R}_f$ the position of the projectile with respect to the same origin after the collision; $\chi^-(\boldsymbol{k}; \boldsymbol{r})$ represents a final continuum wave function ($E > 0$) for the emitted electron with a determined momentum $\boldsymbol{k}$ subject to the potential $V_{\mathrm{moli}}(\boldsymbol{r})$, $C^-(\boldsymbol{K}_f, \boldsymbol{R}_f)$, $C^-(\boldsymbol{k}_{e\mathrm{P}}, \boldsymbol{R}_f - \boldsymbol{r})$ are the Coulombian distortions for the internuclear interaction and the emitted electron-projectile subsystem, respectively. The interaction potential V_{I} is given by the non-resolved part of the Hamiltonian by the initial state:

$$V_{\mathrm{I}}(\boldsymbol{R}_i, \boldsymbol{r}) = -\frac{Z_{\mathrm{P}}}{|\boldsymbol{r} - \boldsymbol{R}_i|} - Z_{\mathrm{P}} V_{\mathrm{moli}}(\boldsymbol{R}_i). \tag{7}$$

We do not use the real anisotropic potential $V_{\mathrm{moli}}(\boldsymbol{r})$ shown in (1) but a radial $U_i(r)$ resulting from its angular integration instead:

$$U_i(r) = \frac{1}{4\pi}\int_{4\pi} \mathrm{d}\Omega\, V_{\mathrm{moli}}(\boldsymbol{r}). \tag{8}$$

As a result, the emitted electron sees the nuclear charge of the central atom (that for the water molecule would be +8) in the limit $r \to 0$, and the asymptotic charge $Z_{\mathrm{asint}} = +1$ as $r \to \infty$. The introduction of this form for the potential seen by the emitted electron, strongly influences the way in which the electron is attracted by the parent molecular ion while in the reaction region compared to the asymptotic form Z_{asint}/r. Such a description is considered to be much more appropriate and is expected to play a clear role in the angular distributions by affecting the shape and intensity of the denominated 'recoil peak'. This structure, represents second order collisions between the emitted electron and the molecular parent ion and gains importance as the emitted electron momentum k_e is greater than the momentum transferred by the projectile (q). In addition, we recall that future experiments with oriented molecules will probably face theoreticians with the need of developing a full anisotropic treatment for the emitted electron-molecular ion potential.

The FDCS for a particular orientation of the water molecule is then a function of the three Euler angles (α, β, γ),

$$\frac{\mathrm{d}^8\sigma}{\mathrm{d}^2\boldsymbol{q}_\perp\,\mathrm{d}^3\boldsymbol{k}\,\mathrm{d}\alpha\,\mathrm{d}\beta\,\mathrm{d}\gamma} = (2\pi)^4 N_e \frac{\mu_{\mathrm{I}e}\mu_{\mathrm{PT}}^2}{K_i K_f} |T_{fi}(\boldsymbol{q}, \boldsymbol{k}, \alpha, \beta, \gamma)|^2. \tag{9}$$

Here, N_e is the number of electrons of the molecular orbital under consideration, and $\mu_{\mathrm{I}e}$, μ_{PT} are the reduced electron–target and projectile–target masses:

$$\mu_{\mathrm{I}e} = \frac{M_{\mathrm{I}}}{M_{\mathrm{I}} + 1} \tag{10}$$

$$\mu_{\mathrm{PT}} = \frac{M_{\mathrm{P}}(M_{\mathrm{I}} + 1)}{M_{\mathrm{P}} + M_{\mathrm{I}} + 1}. \tag{11}$$

If we work in terms of the rotational sudden approximation, we expect the molecular orientation in space to remain constant during the time the collision takes place. Furthermore, the molecular Euler angles are randomly distributed. Then, in order to obtain the FDCS we must average equation (9) over the Euler angles (α, β, γ):

$$\frac{\mathrm{d}^5\sigma}{\mathrm{d}^2\boldsymbol{q}_\perp \mathrm{d}^3\boldsymbol{k}} = \frac{1}{8\pi^2}\int_0^\pi \sin\beta\,\mathrm{d}\beta \int_0^{2\pi}\mathrm{d}\alpha \int_0^{2\pi}\mathrm{d}\gamma \times \frac{\mathrm{d}^8\sigma}{\mathrm{d}^2\boldsymbol{q}_\perp\,\mathrm{d}^3\boldsymbol{k}\,\mathrm{d}\alpha\,\mathrm{d}\beta\,\mathrm{d}\gamma}. \tag{12}$$

We refer the reader to our previous article [43] for more specific details on the calculation procedure of the FDCS including the averaging procedure over the molecular orientation and the way in which the partial wave analysis is handled.

3. Results

We have calculated fully differential single ionization cross sections for collisions of H^+, $\bar{p}^-$ and He^{2+} on H_2O initially in its electronic and vibrational ground state. We have also calculated the doubly differential cross sections for the collision with He^{2+} making a numerical integration of the projectile deflection variables φ_p and q. For that goal we repeated the calculation of the FDCS in a grid of about 23 (depending on which orbital) values for the transferred

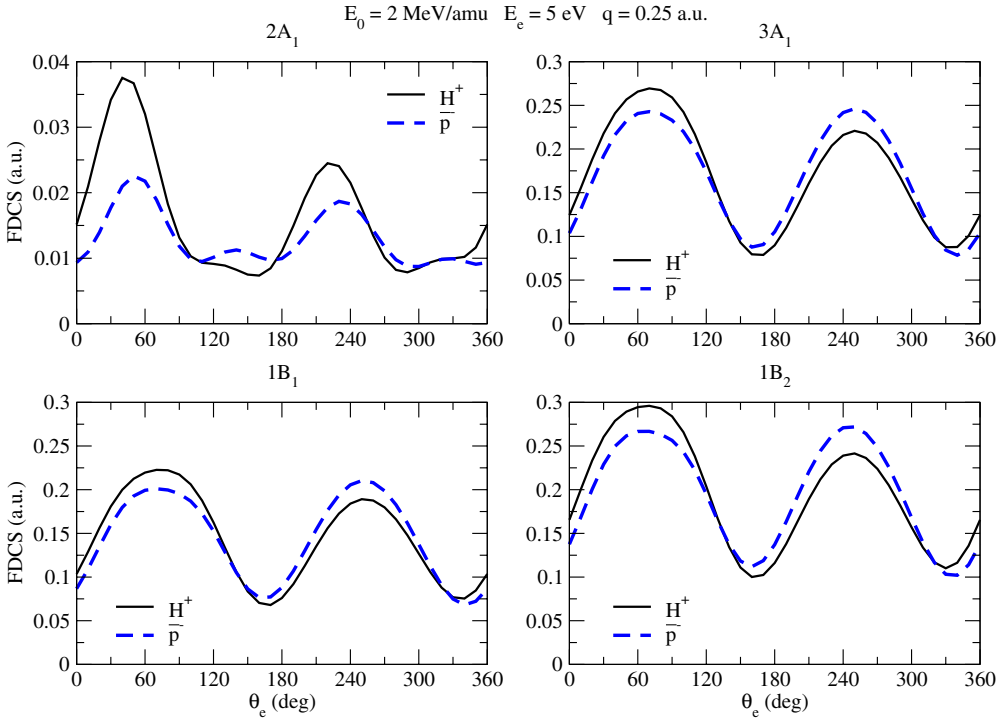

Figure 1. FDCS $\frac{d^5\sigma}{d^2q_\perp d^3k_e}$ for the single ionization of H_2O by H^+ (full line) and $\bar{p}^-$ (dashed line) impact versus the in-plane electron emission θ_e for an impact energy of $E_0 = 2$ MeV amu^{-1}, an electron emission energy of $E_e = 5$ eV, and a transferred momentum $q = 0.25$ au. The four relevant orbitals of the molecule are shown individually.

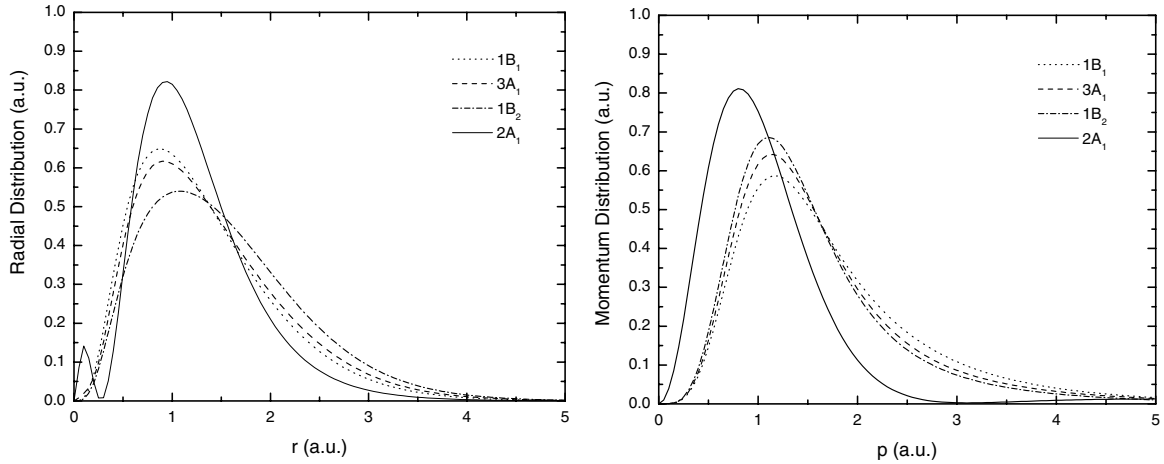

Figure 2. Angularly integrated electronic radial and momentum distributions for the molecular orbitals under consideration.

momentum from $q = K_i - K_f$ to $q = 2.0$ and 15 values for the azimuthal deflection angle between $\varphi_p = 0$ and $\varphi_p = \pi$, the FDCS for the third and fourth quadrant of φ_p were calculated by taking into account the symmetry of the collision. The calculations have been performed at an impact energy of 2 MeV amu^{-1}, and for the FDCS we have considered electron emission energies of 5 and 10 eV and transferred momentum values of 0.25, 0.5 and 0.75 au. In all cases (shown in figures 1–6) the analysis has been restricted to the coplanar geometry in which the momenta of all the particles in the final channel live in the plane defined by $\boldsymbol{K}_i$ and $\boldsymbol{K}_f$. The angle θ_e is the emission angle of the electron in the collision plane measured clockwise from the beam direction. The projectiles are deflected counter clockwise.

In figure 1, we show the FDCS for single ionization of H_2O by H^+ and $\bar{p}^-$ impact. The emitted electron energy is 5 eV and the momentum transferred by the projectile is $q = 0.25$. It can be seen that for the lesser bound molecular orbitals, the typical two-lobe structure appearing in single ionization of hydrogen and helium by ion and electron impact becomes evident. Furthermore, we notice that for these emission geometries, the binary peak is more intense for proton impact while the recoil peak is more intense for $\bar{p}^-$ impact. This can be expected based on the simple postcollisional influence of the receding projectile.

For the $2A_1$ orbital, the binary to recoil peak ratio is also larger for proton impact. However, we note that the angular distributions are not as spread as those previously described.

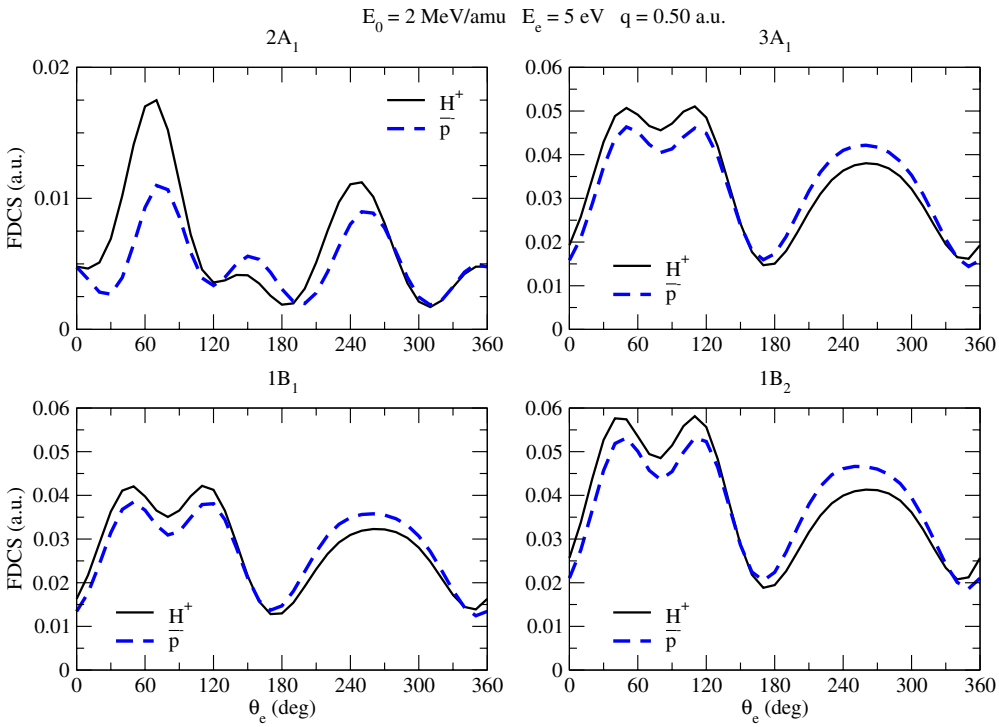

Figure 3. FDCS $\frac{d^5\sigma}{d^2q_\perp d^3k_e}$ for the single ionization of H_2O by H^+ (full line) and $\bar{p}^-$ (dashed line) impact at an energy of $E_0 = 2$ MeV amu^{-1}, an electron emission energy of $E_e = 5$ eV and a transferred momentum $q = 0.50$ au. The four relevant orbitals of the molecule are shown individually.

Furthermore, the FDCS for proton impact seems to be more intense than that of $\bar{p}^-$ impact over the whole angular range. To understand these features, in figure 2 we present the electronic radial and momentum distributions (angularly integrated) for the different orbitals under consideration. It can be seen that the radial distribution for the $2A_1$ orbital clearly shows the footprints of the dominant 2s component which leads to a nodal structure at about 0.25 au and a more compressed distribution than those corresponding to the other orbitals. However, it is in the momentum distribution where the most noticeable difference is found. The $2A_1$ orbital presents a more localized distribution, which leads to narrower structures in the FDCS. Besides, the projectile needs to transfer a larger amount of momentum to ionize an electron from this inner orbital. It is then expected that the ionization channel for this orbital will be fed from low angular momenta (which classically would correspond to inner impact parameters) compared to the lesser bound orbitals. This physical picture leads to the expectation of a greater ionization probability for proton impact compared to the antiproton impact case in which the electron is pushed against the parent molecular ion by the receding projectile.

Similar situations are illustrated in figures 3 and 4 for $q =$ 0.5 and 0.75 au, respectively. Interestingly, for these collision geometries, the lesser bound molecular orbitals clearly exhibit a drastic change in their angular patterns. The binaries as well as recoil peaks are two-peak structures that can be associated to the p-nature of some of the Slaters which conform each molecular orbital. In the present case, for low q values the angular distributions lead to the typical two-peak (binary and recoil) structure as obtained for H and He targets. On the other hand, as the momentum transfer increases, the p-nature of the initial state leads to a clear splitting on each peak as can be inferred from figures 3 and 4, getting a two peak-structure associated to either the binary or recoil structures. Such a behaviour is in agreement with recent calculations and experiments related to the single ionization of Ar(3p) by positrons and electrons [46, 47], where a similar dependence of the binary peak profile with the transferred momentum q has been inferred. As in figure 1, we note that for the more tightly bound orbital under consideration, the proton impact FDCS leads to more intense results compared to the antiproton impact case.

In figures 5 and 6 we show the single ionization FDCS for 2 MeV amu^{-1} He^{2+} impact and an electron emission energy of 5 eV and 10 eV, respectively. The FDCS corresponding to the different orbitals under consideration are shown for three different projectile momentum transfers. Trends observed are similar to those described for proton impact in figures 1, 3 and 4: the binary peak splits in two for increasing projectile momentum transfers. The inner orbital provides more localized structures compared to the lesser bound orbitals, which spread over a larger angular range.

We now turn our attention to the doubly differential cross sections which are given by

$$\frac{d^3\sigma}{dE_e\, d\Omega_e} = \frac{1}{2K_i^2}\int_0^{2\pi} d\varphi_p \int_{K_i-K_f}^{K_i+K_f} dq \times q\left(K_i^2 + K_f^2 - q^2\right)k_e \frac{d^5\sigma}{d^2\boldsymbol{q}_\perp d^3\boldsymbol{k}}. \quad (13)$$

In figures 7 and 8, we show the DDCS for the same collision system for an impact energy of 2 and 6 MeV amu^{-1}, respectively. Electron emission energies of $E_e = 5$ and 10 eV

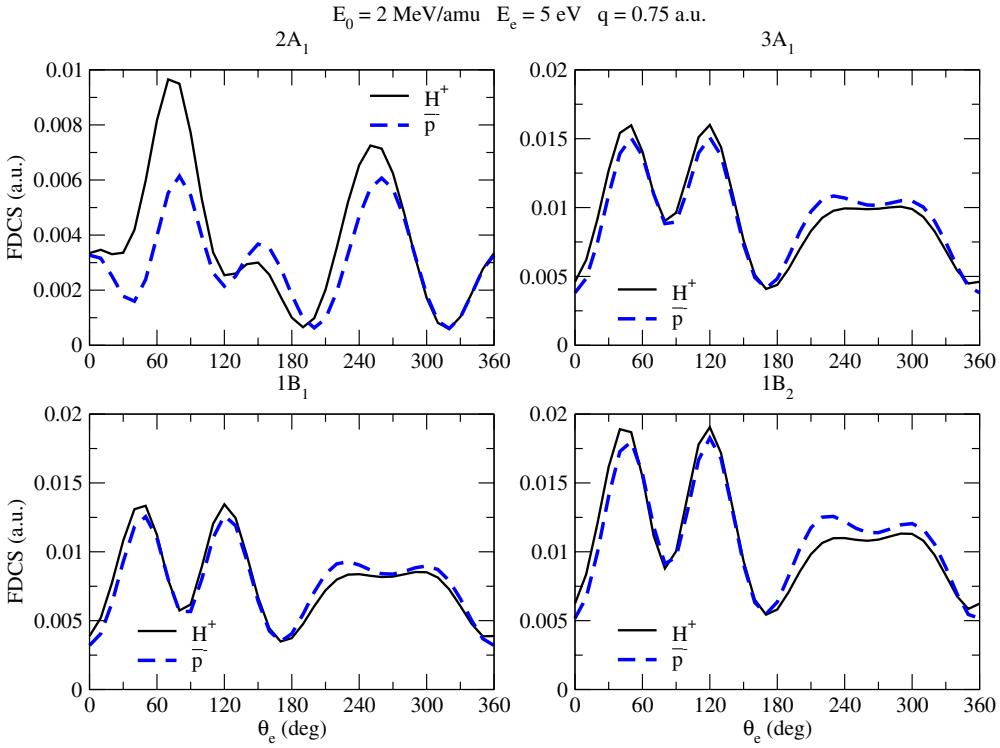

Figure 4. FDCS $\frac{d^5\sigma}{d^2q_\perp d^3k_e}$ for the single ionization of H_2O by H^+ (full line) and $\bar{p}^-$ (dashed line) impact at an energy of $E_0 = 2$ MeV amu^{-1}, an electron emission energy of $E_e = 5$ eV and a transferred momentum $q = 0.75$ au. The four relevant orbitals of the molecule are shown individually.

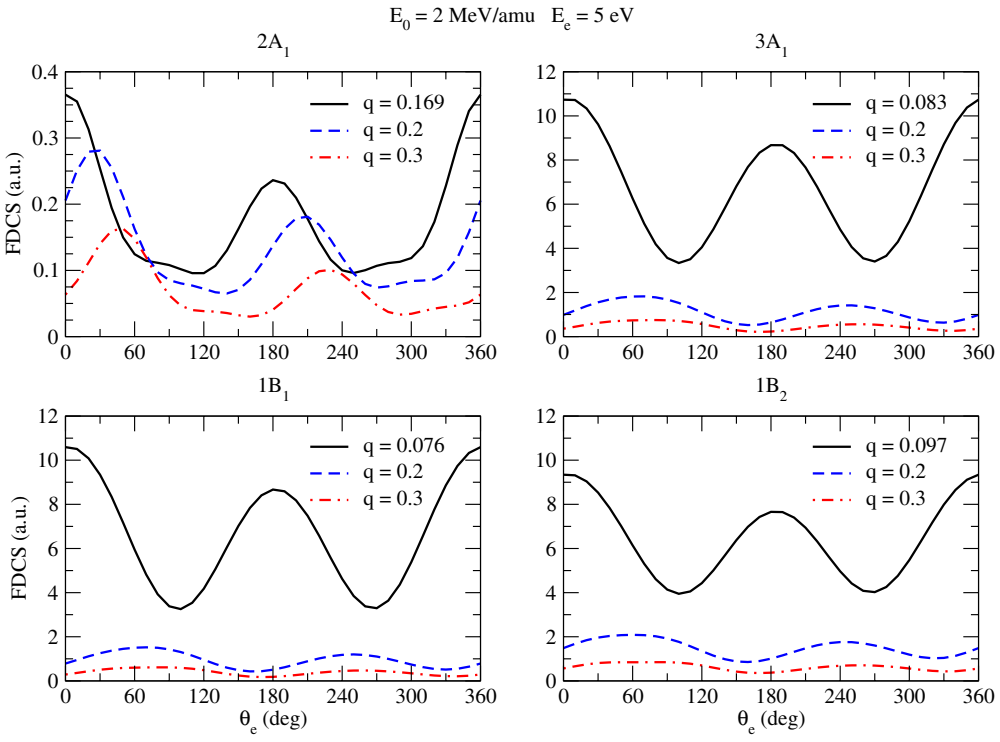

Figure 5. FDCS $\frac{d^5\sigma}{d^2q_\perp d^3k_e}$ for the single ionization of H_2O by He^{2+} impact at an energy of $E_0 = 2$ MeV amu^{-1}, an electron emission energy of $E_e = 5$ eV and three values of the transferred momentum $q = K_i - K_f$, 0.2, 0.3 au. The four relevant orbitals of the molecule are shown individually.

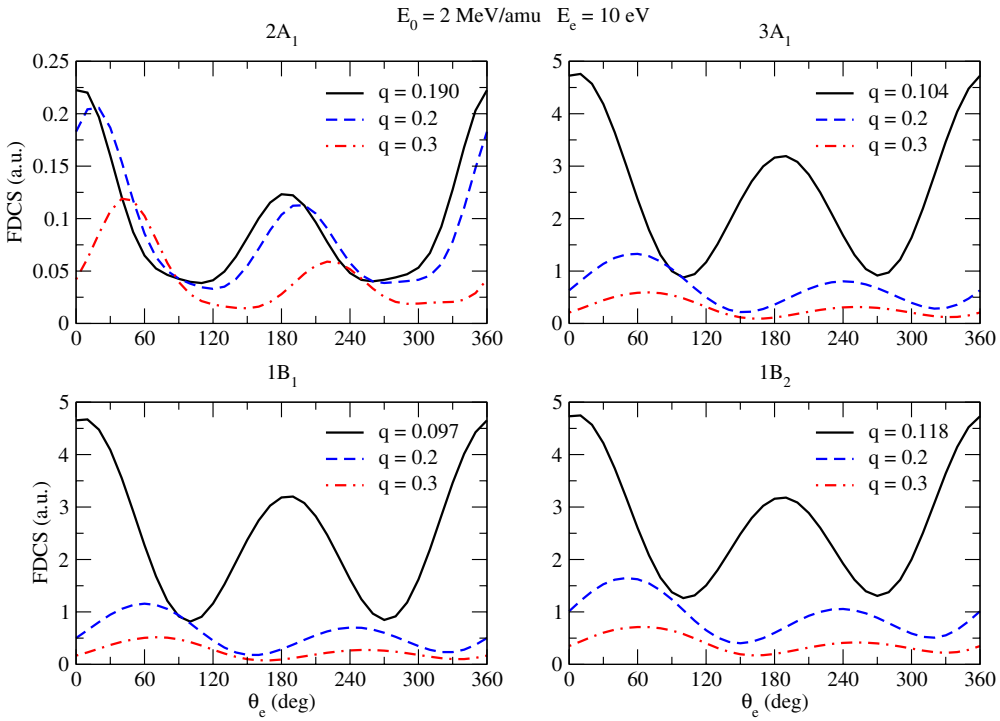

Figure 6. FDCS $\frac{d^5\sigma}{d^2q_\perp d^3k_e}$ for the single ionization of H_2O by He^{2+} impact at an energy of $E_0 = 2$ MeV amu^{-1}, an electron emission energy of $E_e = 10$ eV and three values of the transferred momentum $q = K_i - K_f$, 0.2, 0.3 au. The four relevant orbitals of the molecule are shown individually.

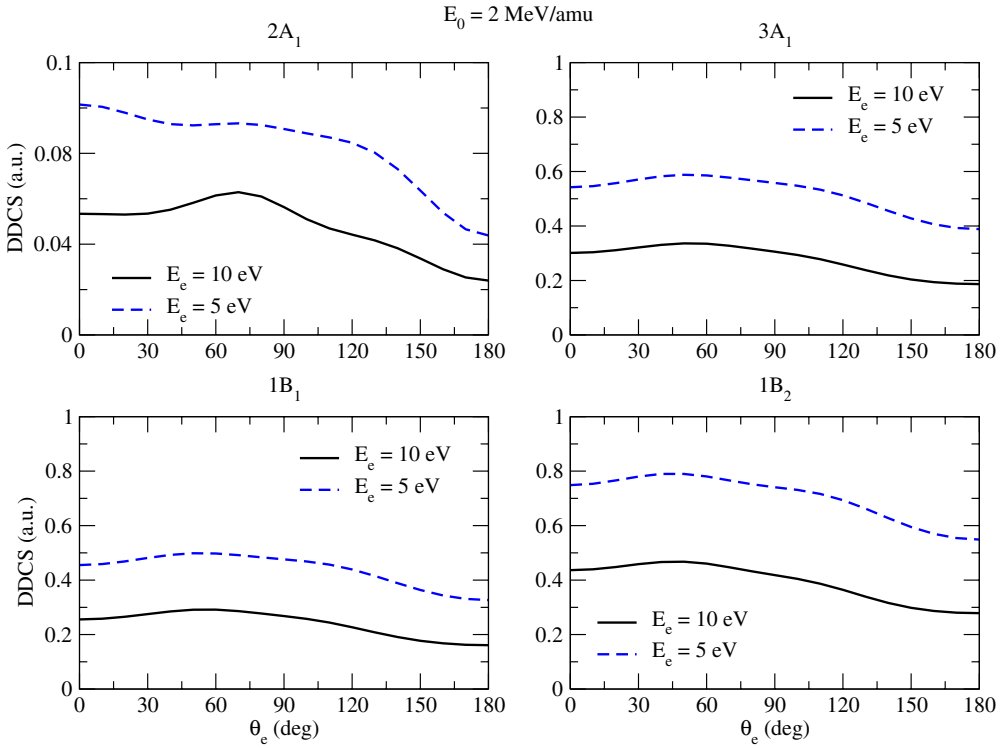

Figure 7. Projectile angle integrated DDCS $\frac{d^3\sigma}{dE_e d\Omega_e}$ for the single ionization of H_2O by He^{2+} impact at an energy of $E_0 = 2$ MeV amu^{-1}, an electron emission energy of $E_e = 5$ and 10 eV. The four relevant orbitals of the molecule are shown individually.

are explicitly considered for the case of $E_0 = 2$ MeV amu^{-1}, while for $E_0 = 6$ MeV amu^{-1} we only considered the electron emission energy $E_e = 10$ eV. In all cases, the DDCS are shown as a function of the electron ejection angle counted clockwise. For the lesser bound orbitals, we observe that the distributions are nearly isotropic with a maximum around 60°.

So far, we have been mainly concerned with the analysis of the profiles exhibited by the FDCS and DDCS for the different

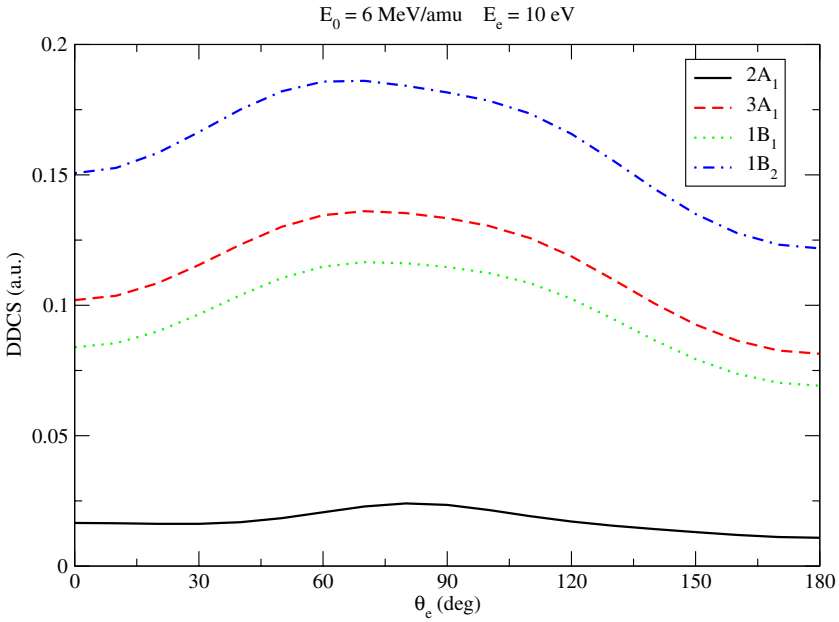

Figure 8. Projectile angle integrated DDCS $\frac{d^3\sigma}{dE_e d\Omega_e}$ for the single ionization of H_2O by He^{2+} impact at an energy of $E_0 = 6$ MeV amu^{-1}, an electron emission energy of 10 eV. The four relevant orbitals of the molecule are shown individually.

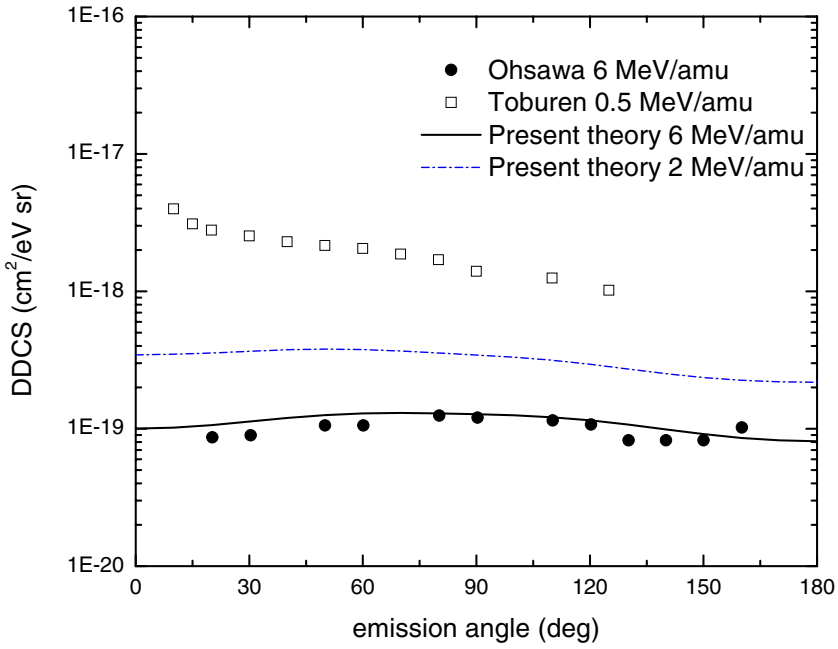

Figure 9. Calculated DDCS as a function of electron emission angle at impact energy 2 and 6 MeV amu^{-1} and electron emission energy of 10 eV. (—) present work; (●) 6 MeV amu^{-1} data of Ohsawa *et al* [17]; (□) 0.5 MeV amu^{-1} data of Toburen [50].

orbitals in terms of the electron emission angle. However, to compare to experiments another issue should be considered. Orbitals with similar ionization potentials might individually contribute to the ionization channel for a given scattering angle or, in impact parameter methods, for a given impact parameter. In this sense, the single ionization probability from one explicit orbital should take into account that no other electron is simultaneously removed from any other competing orbital. In impact parameter methods, the contribution from a given orbital to the ionization channel is then given by the probability to ionize one electron from that orbital, times the probability of no-electron removal from the remaining orbitals (see for example [36]).

Alternatively, in the present context we follow the proton impact ionization studies on H_2O molecules by Luna *et al* [19] together with their reported dissociation probabilities [48] and we consider branching ratios of 0.32 for the $1B_1$ and $3A_1$ orbitals and 0.36 for the $1B_2$ orbital. We note that a similar strategy has been used in recent years to address single electron capture processes on H_2O molecules by bare ions at low impact energies [49]. The resulting DDCS is shown in figure 9 and is in very good agreement with the data from Ohsawa *et al* [17], which predict a practically isotropic behaviour as a function

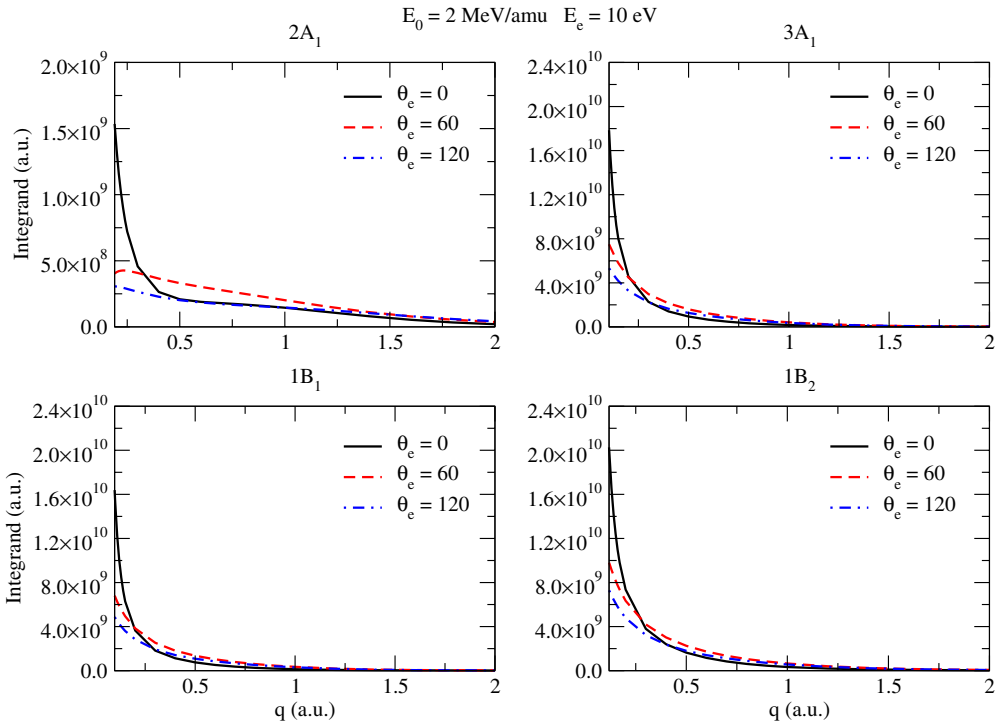

Figure 10. Integrand of equation (13) for the single ionization of H_2O by He^{2+} impact at an energy of $E_0 = 2$ MeV amu^{-1}, an electron emission energy of $E_e = 10$ eV, and three values of the electron in plane ejection angle of $\theta_e = 0, 60^\circ, 120^\circ$. The four relevant orbitals of the molecule are shown individually.

Table 5. Electron ejection angles integrated SDCS $\frac{d\sigma}{dE_e}$ (au) for the single ionization of H_2O by He^{2+} impact at an energy of $E_0 = 2$ and 6 MeV amu^{-1}, and electron emission energies of $E_e = 5$ and 10 eV. The four relevant orbitals of the molecule are shown individually.

$E_0 = 2$ MeV amu^{-1}				
E_e (eV)	$2A_1$	$3A_1$	$1B_1$	$1B_2$
5	1.0858	6.7408	5.7367	9.0845
10	0.6406	3.6306	3.1628	5.0725
$E_0 = 6$ MeV amu^{-1}				
10	0.236 592	1.528 81	1.307 47	2.133 55

of the emission angle. In the figure, we also add the calculated DDCS at 2 MeV amu^{-1} and incorporate the low energy data of Toburen to help visualize how the DDCS magnitudes decrease as the impact energy increases [50].

In figure 10 we show the integrand of the DDCS (13) after performing the first integral in the azimuthal angle of the projectile. Three electron emission angles are explicitly shown. The integral is converged for a value of the transferred momentum of $q = 2$ au while the initial momentum values $K_i = 53\,747$ au.

Once the molecular orientation and the projectile deflection angles are averaged, the system gains the cylindrical symmetry. As a result, the DDCS shown in figure 7 is symmetrical with respect to the 180° angle. We can calculate then the single differential cross section (SDCS) with a single integral using this symmetry as

$$\frac{d\sigma}{dE_e} = 2\pi \int_0^\pi \sin\theta_e \, d\theta_e \, \frac{d^3\sigma}{dE_e d\Omega_e}. \qquad (14)$$

In table 5 we show the calculated SDCS for the two energies for the ejected electron calculated in present work. After using the above mentioned branching ratios, the estimated SDCS read at 2 MeV amu^{-1}, 7.47×10^{-18} cm^2 eV^{-1} (5 eV) and 4.11×10^{-18} cm^2 eV^{-1} (10 eV). On the other hand, at 6 MeV amu^{-1} impact energy and 10 eV emission energy, the estimated SDCS reads 1.72×10^{-18} cm^2 eV^{-1}.

4. Conclusions

In this work we have studied the single ionization of the water molecule at the fully and doubly differential level. The present study has been performed by using a recently developed distorted wave model which considers a model central potential for the emitted electron-molecular ion interaction.

The present results suggest that for low momentum transfers and low energy emitted electrons, the typical two-lobe (binary-recoil) profile is obtained. As the momentum transfer increases, these structures evolve into more complex ones, splitting due to the *p*-character of the molecular orbitals under study. These results are in agreement with recent experimental and theoretical studies on fully differential cross section (FDCS) for the single ionization of Ar(3p) by electrons and positrons [46, 47].

For the inner orbital under consideration ($2A_1$), we noticed that the calculated FDCS present narrower structures compared to those obtained for the lesser bound molecular orbitals. We ascribe this feature to the more localized electronic momentum distribution.

We have also calculated the double differential cross section for the collision of He^{2+} with H_2O, from the different molecular orbitals finding very good agreement with the

experimental data of Ohsawa *et al* at an impact energy of 6 MeV amu^{-1}. To achieve convergence in the integration procedures, we needed a grid of 23 values of the transferred momentum q, depending on the orbital, and 15 values of the azimuthal deflection angle of the projectile φ_p for each point of the graphic 7. That took two months of calculation for each electron energy occupying 400 nodes on the computation cluster at IPP-Garching. This proves that the present model, conceived to improve the description at the fully differential level, is ineffective to obtain integrated values, and absolutely not usable to get the total cross sections. Other methods, like classical trajectory Monte Carlo method, proved through the years to be effective and fast to provide integrated cross sections while computation time drastically increases as we move to fully differential data. In this sense, complementary strategies should be conceived to identify and fill the gaps in ionization cross section databases that could be relevant in different fields.

We have concentrated on collision and emission energies that are accessible with the cold target recoil ion momentum spectroscopy (COLTRIMS) technique (low q values, low-energy electron emission) although water is not an easy target to deal with COLTRIMS. Experiments recently performed with such a reaction microscope, employing a water target in the vapour phase at a target temperature of 383 K, involved the measurement of the kinetic energy release of the ionic fragments [51]. We note, on the other hand, that FDCS for the single ionization of water molecules by electrons have been measured in recent years using an electron coincidence spectrometer [52]. In this sense, we hope that experimental data for the single ionization of water by ion impact will be available in the next few years. That would help us to further test and refine the theoretical models currently under use and provide reliable data that could fill the gaps in cross section databases for medical and astrophysical applications.

Acknowledgments

This work has been supported by the Universidad Nacional del Sur (project no PGI 24/F059), and Consejo Nacional de Investigaciones Científicas y Técnicas, Argentina (project no PIP 112-201101-00749). The calculations were carried out in the TOK-Linux cluster in the Max Plank Institut für Plasmaphysik in Garching and computing clusters of APAP project in the University of Strathclyde. We thank Professor L Toburen for sending us his data in tabular form.

References

[1] Stolterfoht N, Dubois R D and Rivarola R D 1997 *Electron Emission in Heavy Ion-Atom Collisions* (New York: Springer)
[2] Rescigno T N, Baertschy M, Isaacs W A and McCurdy C W 1999 *Science* **286** 2474
[3] Baertschy M, Rescigno T N and McCurdy C W 2001 *Phys. Rev.* A **64** 022709
[4] Bray I, Fursa D V, Kadyrov A S and Stelbovics A T 2010 *Phys. Rev.* A **81** 062704
[5] Amaldi U and Kraft G 2005 *Rep. Prog. Phys.* **68** 1861
[6] Ulrich J *et al* 1997 *J. Phys. B: At. Mol. Opt. Phys.* **30** 2917
[7] Dörner R *et al* 1994 *Phys. Rev. Lett.* **72** 3166–9
[8] Moshammer R, Ullrich J, Unverzagt M, Schmitt W and Schmidt-Böcking B 1996 *Nucl. Instrum. Methods Phys. Res.* B **108** 425–45
[9] Dörner R *et al* 1998 *Phys. Rev.* A **57** 1074–1090
[10] Dörner R, Mergel V, Spielberger L, Jagutzki O, Ullrich J and Schmidt-Böcking H 1998 *Phys. Rev.* A **57** 312–7
[11] Mergel V *et al* 2001 *Phys. Rev. Lett.* **86** 2257–60
[12] Dörn A *et al* 2001 *Phys. Rev. Lett.* **86** 3755–8
[13] Nguyen H, Brédy R, Camp H A, Awata T and DePaola B D 2004 *Phys. Rev.* A **70** 032704
[14] Schmidt L P H *et al* 2007 *Phys. Rev.* A **76** 012703
[15] Guan X and Bartschat K 2009 *Phys. Rev. Lett.* **103** 213201
[16] Alessi M, Otranto S and Focke P 2011 *Phys. Rev.* A **83** 014701
[17] Ohsawa D, Sato Y, Okada Y, Shevelko V P and Soga F 2005 *Phys. Rev.* A **72** 062710
[18] García P M Y, Sigaud G M, Luna H, Santos A C F, Montenegro E C and Shah M B 2008 *Phys. Rev.* A **77** 052708
[19] Luna H *et al* 2007 *Phys. Rev.* A **75** 042711
[20] Martin S *et al* 2008 *Phys. Rev.* A **77** 062513
[21] Alessi M, Cariatore N D, Focke P and Otranto S 2012 *Phys. Rev.* A **85** 042704
[22] Hoener M *et al* 2008 *Phys. Rev.* A **78** 021201
[23] Champion C, Dal Cappello C, Houamer S and Mansouri A 2006 *Phys. Rev.* A **73** 012717
[24] Champion C, Boudrioua O, Dal Cappello C, Sato Y and Ohsawa D 2007 *Phys. Rev.* A **75** 032724
[25] Dal Cappello C, Champion C, Boudrioua O, Lekadir H, Sato Y and Ohsawa D 2009 *Nucl. Instrum. Methods Phys. Res.* B **267** 781–90
[26] Martínez S, Otranto S and Garibotti C R 2008 *Phys. Rev.* A **77** 024701
[27] Godunov A L, Whelan C T and Walters H R J 2008 *Phys. Rev.* A **78** 012714
[28] Fiol J and Olson R E 2002 *J. Phys. B: At. Mol. Opt. Phys.* **35** 1759
[29] Fiol J, Otranto S and Olson R E 2006 *J. Phys. B: At. Mol. Opt. Phys.* **39** L285
[30] Ohsawa D, Tawara H, Okada T, Soga F, Galassi M E and Rivarola R D 2012 *J. Phys.: Conf. Ser.* **388** 102029
[31] Champion C, Galassi M E, Weck P F, Fojón O, Hanssen J and Rivarola R D 2012 *J. Phys.: Conf. Ser.* **388** 102003
[32] Fiol J and Olson R E 2004 *J. Phys. B: At. Mol. Opt. Phys.* **37** 3947
[33] Otranto S, Olson R E and Fiol J 2006 *J. Phys. B: At. Mol. Opt. Phys.* **39** L175–83
[34] Errea L F, Illescas C, Méndez L, Pons B, Rabadán I and Riera A 2007 *Phys. Rev.* A **76** 040701
[35] Illescas C, Errea L F, Méndez L, Pons B and Rabadán I 2012 *J. Phys.: Conf. Ser.* **388** 102007
[36] Illescas C, Errea L F, Méndez L, Pons B, Rabadán I and Riera A 2011 *Phys. Rev.* A **83** 052704
[37] Lüdde H J, Spranger T, Horbatsch M and Kirchner T 2009 *Phys. Rev.* A **80** 060702
[38] Dubois A, Carniato S, Fainstein P D and Hanssen J P 2011 *Phys. Rev.* A **84** 012708
[39] Martínez P, Errea L F, Méndez L and Rabadán I 2012 *J. Phys.: Conf. Ser.* **388** 102034
[40] Kirchner T, Murakami M, Horbatsch M and Lüdde H J 2012 *J. Phys.: Conf. Ser.* **388** 012038
[41] Champion C, Hanssen J and Hervieux P A 2001 *Phys. Rev.* A **63** 052720
[42] Champion C, Hanssen J and Hervieux P A 2005 *Phys. Rev.* A **72** 059906
[43] Fernández-Menchero L and Otranto S 2010 *Phys. Rev.* A **82** 022712
[44] Tóth I and Nagy L 2010 *J. Phys B: At. Mol. Opt. Phys.* **43** 135204

[45] Moccia R 1964 *J. Chem. Phys.* **40** 2164
[46] de Lucio O G, Otranto S, Olson R E and DuBois R D 2010 *Phys. Rev. Lett.* **104** 163201
[47] Otranto S and Olson R E 2009 *Phys. Rev.* A **80** 012714
[48] Montenegro E C 2009 *J. Phys.: Conf. Ser.* **194** 012049
[49] Otranto S and Olson R E 2008 *Phys. Rev.* A **77** 022709
[50] Toburen L H 2013 private communication
[51] Sann H *et al* 2011 *Phys. Rev. Lett.* **106** 133001
[52] Milne-Brownlie D S, Cavanagh S J, Lohmann B, Champion C, Hervieux P A and Hanssen J 2004 *Phys. Rev.* A **69** 032701